Dissipative Laser-Driven Hydrogen-Bond Dynamics in Deuterated *o*-Phthalic Acid Monomethylester

O. Kühn

Institut für Chemie, Physikalische und Theoretische Chemie, Freie Universität Berlin, Takustrasse 3, D-14195 Berlin

Received: April 17, 2002; In Final Form: June 6, 2002

The intramolecular nuclear wave packet dynamics of carboxy-deuterated *o*-phthalic acid monomethylester following ultrafast excitation of the OD stretching vibration in the hydrogen bond is investigated. On the basis of quantum chemical calculations of the normal modes as well as the anharmonicities, a three-dimensional model is proposed comprising the OD stretching and bending as well as a low-frequency mode which modulates the hydrogen bond geometry. The interaction with the remaining intramolecular and solvent degrees of freedom is incorporated within a quantum master equation formulation. The linear absorption spectrum is shown to be dominated by a Fermi resonance, with the actual line widths depending on pure dephasing as well as on a fourth-order relaxation process. The latter involves two intramolecular vibrational quanta plus a solvent phonon. It proves to be vital for the explanation of the very fast relaxation of the fundamental OD stretching excitation. Further, it is shown that in the OD ground state vibrational coherences with respect to the low-frequency mode are completely dephased only after about 2 ps. These results are discussed in the context of recent infrared pump−probe and four-wave-mixing experiments.

1. Introduction

Hydrogen bonds A−H···B manifest themselves in a red-shift and a broadening of the infrared (IR) absorption band as compared to the free A−H vibration.[1] In addition a peculiar substructure often indicates the anharmonic coupling between the A−H vibration and other intramolecular modes such as the low-frequency A···B vibration. In the condensed phase the details of the spectrum are usually masked by the broadening due to intermolecular interactions. This situation renders the interpretation based solely on the linear absorption spectrum difficult and nonlinear-IR spectroscopy has to be employed[2−15] Recently, Stenger et al.[8,9,14] reported femtosecond IR pump−probe experiments on carboxy-deuterated *o*-phthalic acid monomethylester (PMME-D) in C_2Cl_4 which exhibits an intramolecular H-bond of medium strength (cf. Figure 1). From the decay of the excited state absorption of the OD stretching vibration, the relaxation dynamics of the fundamental transition could be characterized by a time scale of about 400 fs. A second time scale of 20 ps was attributed to vibrational cooling of the anharmonically coupled modes in the OD vibrational ground state. The most striking observation, however, was an oscillatory component in the signal, surviving for about 1.5 ps and being attributed to underdamped wave packet motion with respect to a low-frequency mode (about 100 cm^{-1}) modulating the H-bond geometry. This is a clear manifestation of the effect of anharmonic couplings on the H-bond dynamics which is hidden under the broad absorption band (cf. Figure 3 below). In addition, photon echo studies for the normal species PMME-H in ref 12 revealed an extremely short dephasing time of about 40 fs for the OH fundamental transition.

In the theoretical literature the line shape of A−H···B hydrogen bonds is usually discussed in terms of a fast mode, ν_{A-H}, being anharmonically coupled to a slow mode, $\nu_{A..B}$. After performing an adiabatic separation (second Born−Oppenheimer approximation) an analytical treatment becomes possible in close analogy to optical spectroscopy of electronic transitions.[16] In particular, Franck−Condon type vibrational progressions are obtained from combination transitions involving the low-frequency mode.[17] The dephasing of the ν_{OD} fundamental transition has been modeled assuming a direct coupling of the related dipole moment to the fluctuating field of the surroundings[18] or an indirect coupling via the damping of the low-frequency mode described either quantum mechanically[19,20] or via a stochastic process.[21]

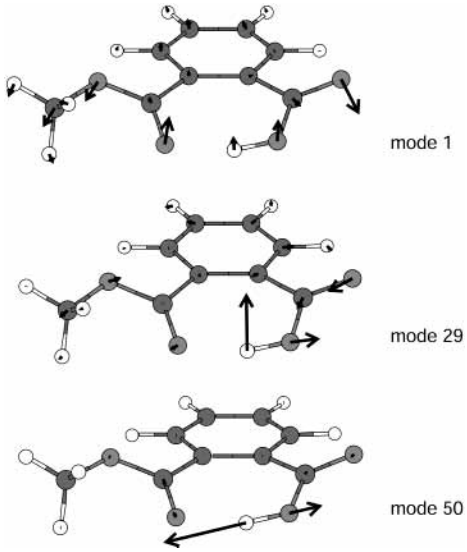

Figure 1. Displacement vectors for those 3 normal modes of PMME which define the relevant system. Mode ν_{50} is the OD-stretching, ν_{29} the out-of-plane O−D-O bending, and ν_1 an out-of-plane torsional motion. The O−O distance of 2.56 Å and the single minimum anharmonic shape of the potential surface indicate a H-bond of moderate strength in this system. The quantum chemical calculations were performed using the DFT/B3LYP level of theory with a Gaussian 6-31+G(d,p) basis set.

10.1021/jp0209852 CCC: $22.00
Published on Web 07/20/2002

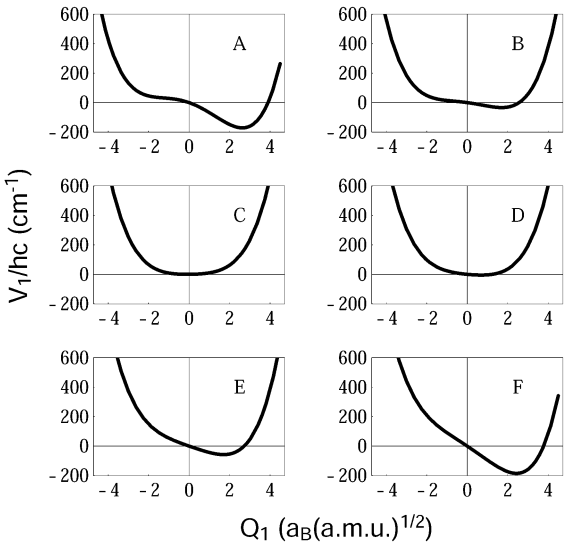

Figure 2. Potential energy surface$V_1(Q_{50}, Q_1)$ for $Q_{50} = -0.35$ (A), -0.23 (B), 0 (C), 0.23 (D), 0.5 (E), and $0.7a_B\sqrt{\text{amu}}$ (F).

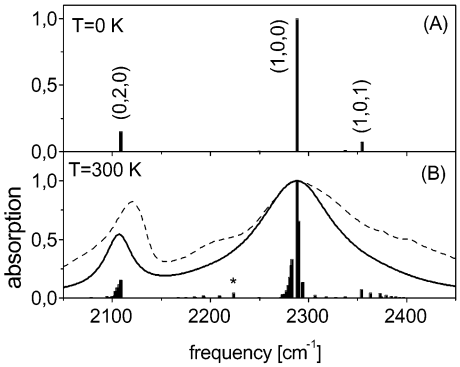

Figure 3. Linear absorption spectrum of PMME-D in the OD stretching region: (A) zero temperature (gas phase) stick spectrum of the relevant system. (B) $T = 300$ K stick spectrum together with the condensed phase spectrum according to Eq. lorentz (solid line) as well as the experimental spectrum taken from ref 9 (dashed line). The parameters for the system−bath coupling are $g_i^{(I)} = 0.01$, $g_{50}^{(II)} = 0.005$, $g_{1,29}^{(II)} = 0.0001$, $\gamma_{pd} = 0.6\ s^{-1}$, $g^{(III)} = 0.02$, $\omega_c^{(I)}/2\pi c = 100\ cm^{-1}$, and $\omega_c^{(III)}/2\pi c = 250\ cm^{-1}$.

An additional complication arises from the ubiquitous presence of Fermi resonances involving the A−H stretch fundamental and its bending overtone transition. It leads to the appearance of the so-called Evans window separating the two transitions. The most comprehensive study in this respect has been provided by Henri-Rousseau and co-workers who supplemented the above-mentioned two mode quantum model by a Fermi resonance coupling to a bending overtone transition while taking into account the direct dephasing of the bending and stretching modes.[22,23] In doing so they extended earlier relaxation-free work by Witkowski and Wójcik[24] as well as the stochastic description given by Bratos and co-worker for the static modulation limit.[25,26] For an overview see also refs 27 and 28.

In an effort to understand the intramolecular dynamics of PMME-D we have recently combined a full-dimensional reaction surface study with a time-dependent Hartree dynamics simulation in the mean-field[29] and the numerically exact multiconfiguration[30,31] limit. This parameter-free approach was capable of reproducing the periodic low-frequency modulation of the H-bond dynamics. However, the estimated decay time of the OD stretching excitation was about 20 ps. This led to the conclusion that the interaction with the solvent must play an important role for relaxation, e.g., by bridging the gap between otherwise nonresonant intramolecular transitions. Following this idea we will develop a system−bath model of PMME-D in the condensed phase in section 2. This approach combines an accurate description of the relevant degrees of freedom with a perturbational treatment of its interaction with a heat bath, i.e., the remaining intramolecular modes and the solvent. Such a general strategy has been followed, e.g., in refs 32−35. (For an alternative treatment of condensed phase proton-transfer reactions see, e.g., refs 35 and 36.) In section 3 the linear absorption spectrum is discussed and the relevant mechanisms for understanding the line shape are identified. The proposed model is supported by comparing relevant time scales from dissipative quantum dynamics simulations with experimental results[8,9,14] in section 4. Section 5 summarizes our results.

TABLE 1: Normal Modes of PMME-D Which Couple Appreciably to Mode ν_{50} (OD Stretch, cf. Figure 1)[a]

mode	$\omega_i/2\pi c$ (cm^{-1})	$f_i(mE_h/a_B\sqrt{\text{amu}})$
1	**38**	**0.24**
2	72	0.02
7	228	0.31
8	275	−1.06
9	323	0.34
10	357	0.84
11	390	0.31
12	426	0.73
14	488	−1.07
16	*620*	*2.13*
19	692	1.32
21	786	1.79
24	853	−0.31
29	**1043**	**0.64**
38	1306	0.21
39	*1329*	*−1.50*

[a] The forces f_i have been calculated at $Q_{50} = 0.5a_B\sqrt{\text{amu}}$ by performing two additional single-point calculations for structures displaced by $\pm\delta Q_i$. The two modes which have been included into the relevant system are given bold-faced; the two modes entering the fourth-order system−bath coupling are shown in italic.

2. Model Hamiltonian

2.1. Relevant System. The geometry of PMME-D in the electronic ground state has been optimized using the DFT/B3LYP level of theory with a Gaussian 6-31+G(d,p) basis set[37] (for a comparison of DFT and MP2 results, see refs 29 and 30). Because we are interested in the dynamics in the vicinity of the most stable configuration we have chosen to express the system Hamiltonian in terms normal mode coordinates $\{Q_i\}$. The most important coordinate corresponds to the normal mode vibration ν_{50} having essentially OD stretching character as can be seen from Figure 1. Displacing the PMME-D structure along Q_{50} and performing additional single point energy calculations one obtains the anharmonic potential $V_0(Q_{50})$ as well as the related dipole moment d (Q_{50}).

To quantify the anharmonic mode−mode coupling we have calculated the force acting on those normal modes which, according to their displacement vectors, potentially have an influence on the H-bond. The calculations have been performed for an elongated OD bond ($Q_{50} = 0.5a_B\sqrt{\text{amu}}$) by finite differences. The results are compiled in Table 1. The observation of coherent vibrational wave packet dynamics in refs 8 and 9 as well as our previous investigations[29−31] provide evidence that in a reasonable model for the *relevant system* the OD stretching coordinate has to be supplemented by at least a coordinate describing a low-frequency modulation of the H-bond. The

experimental frequency of about 100 cm^{-1} would have suggested that mode ν_2 is strongly coupled (see also discussion in ref 9). Surprisingly, ν_2 has the smallest force in Table 1. On the other hand, exploring the PES along mode ν_1 (cf. Figure 1) we found that in the vicinity of the equilibrium configuration the curvature is much better represented by a harmonic force constant which corresponds to $\nu_1 = 70$ cm^{-1} (see also part C of Figure 2). Therefore, we conclude that mode ν_1 needs to be incorporated into the relevant system.

From Table 1 we notice that the strongest coupling is to mode ν_{16} which corresponds to a bending vibration within the H-bond; the second bending mode is ν_{29}. Because the first overtone of ν_{29} is close to resonance with the OD fundamental transition we will include this mode as the third DOF into the relevant system (see Figure 1). The importance of this type of out-of-plane bending mode has also been emphasized in ref 29. The remaining modes will be considered to be part of the environment in section 2.2, with ν_{16} and also ν_{39} playing an important role in the relaxation dynamics.

For the potential energy surface of the relevant system we have used the following form

$$V(Q_{50},Q_{29},Q_1) = V_0(Q_{50}) + V_1(Q_{50},Q_1) + V_{29}(Q_{50},Q_{29}) \quad (1)$$

Here, $V_0(Q_{50})$, $V_1(Q_{50},Q_1)$, and $V_{29}(Q_{50},Q_{29})$ are the potentials which are obtained when all other coordinates are fixed at their equilibrium positions, e.g., $V_0(Q_{50}) = V(Q_{50},Q_1=0,Q_{29}=0)$. Notice that eq 1 is an approximation since the direct coupling between ν_1 and ν_{29} is not included. This treatment reduces the number of single-point calculations dramatically, i.e., instead of a full three-dimensional (3D) grid only two two-dimensional (2D) grids have to be spanned. Here we used 18 points along Q_{50} and 7−11 points along Q_{29} and Q_1, depending on the shape of the potential. Subsequently the potential surface was fitted to high order polynomials. In Figure 2 we show representative plots of $V_1(Q_{50},Q_1)$. It is interesting to see that the range of validity of the harmonic approximation is rather limited. The anharmonicity of $V_{29}(Q_{50},Q_{29})$ is less striking (not shown).

The interaction of the 3D system with the external electric field $E(t)$ will be included within the dipole approximation via the Hamiltonian

$$H_f(t) = -E(t)d(Q_{50}) \quad (2)$$

Note that the gradient of the dipole moment along Q_{29} and Q_1 is more than an order of magnitude smaller than for Q_{50}, i.e., it can be safely neglected.

The 3D system Hamiltonian $H_{sys} = T_{sys} + V_{sys}$ has been diagonalized using an expansion of the total wave function in terms of zero-order states, $|\varphi_i^{(k)}\rangle$. The latter were defined with respect to the reference potentials $V_0(Q_{50})$, $V_1(Q_{50}=0,Q_1)$, and $V_{29}(Q_{50}=0,Q_{29})$ using the Fourier grid Hamiltonian method.[38] Thus we have for the ath eigenstate

$$|a\rangle = \sum_{ijk} C_{a,ijk}|\varphi_i^{(50)}\rangle|\varphi_j^{(29)}\rangle|\varphi_k^{(1)}\rangle \quad (3)$$

where we employed 5, 8, and 25 basis states for the expansion in Q_{50}, Q_{29}, and Q_1 direction, respectively. This was sufficient to obtain convergence for the lower part of the spectrum up to energies corresponding to the ν_{50} overtone transition at about 4400 cm^{-1}. Transition energies and expansion coefficients of some of the more important eigenstates are summarized in Table 2.

TABLE 2: The Transition Energies and Relevant Expansion Coefficients ($|C_{a,ijk}| > 0.2$ in Equation 3) for Important Eigenstates of the Three-Dimensional System Hamiltonian Are Given Together with Population Relaxation Rates as Well as Full and Pure Coherence Dephasing Rates with Respect to the Ground State (See Discussion in Section 3)

state	$\omega_{a1}/2\pi c$ (cm^{-1})	ijk	$C_{a,ijk}$	$1/R_{aa,aa}$ (ps)	$1/R_{a1,a1}$ (ps)	$1/R^*_{a1,a1}$ (ps)
1	0	0 0 0	0.992	18.9		
2	65	0 0 1	0.984	7.1	0.590	0.626
3	145	0 0 2	0.983	5.4	0.571	0.613
29	2108	1 0 0	−0.328	0.887	0.367	0.468
		0 2 0	0.923			
31	2171	1 0 1	−0.336	0.794	0.346	0.447
		0 2 1	0.903			
34	2250	1 0 2	−0.351	0.728	0.325	0.423
		0 2 2	0.889			
35	2288	1 0 1	0.318	0.322	0.102	0.121
		1 0 0	0.869			
		0 2 0	0.306			
36	2338	1 0 3	−0.366	0.633	0.285	0.372
		0 2 3	0.849			
		0 2 2	0.229			
37	2354	1 0 2	0.280	0.329	0.107	0.128
		1 0 1	0.789			
		1 0 0	−0.348			
		0 2 3	−0.271			
		0 2 1	0.270			
40	2428	1 0 4	0.277	0.345	0.124	0.151
		1 0 3	−0.254			
		1 0 2	0.662			
		1 0 1	−0.319			
		0 2 4	−0.393			
		0 2 3	−0.273			
		0 2 2	0.250			
41	2439	1 0 4	−0.254	0.544	0.224	0.284
		1 0 2	0.451			
		0 2 4	0.792			
42	2518	1 0 4	−0.272	0.310	0.103	0.124
		1 0 3	0.760			
		1 0 2	0.359			
		0 2 4	−0.260			
		0 2 3	0.277			
45	2541	1 0 5	−0.332	0.624	0.278	0.361
		1 0 3	−0.244			
		0 2 5	0.866			
46	2614	1 0 5	0.264	0.306	0.102	0.122
		1 0 4	0.770			
		1 0 3	0.364			
		0 2 5	0.270			
		0 2 4	0.279			

2.2. System−Bath Interaction. The coupling of the 3D relevant system to the remaining intramolecular degrees of freedom, $\{q_m\}$, as well as to those of the solvent, $\{Z_\xi\}$, will be taken into account using the formalism of dissipative quantum dynamics.[16] In particular it will be assumed that the conditions for Markovian dynamics and weak system−(harmonic) bath coupling apply. In view of our previous studies,[29−31] the latter assumption is most likely fulfilled. The validity of the Markov approximation especially for the intramolecular modes is a hypothesis which could be verified at least in principle, e.g., by enlarging the relevant system.

For the system−bath interaction Hamiltonian, we take the standard form[16]

$$H_{SB} = \sum_u K^{(u)}(\{Q_i\})\Phi^{(u)}(\{q_m\},\{Z_\xi\}) \quad (4)$$

with the operators $K^{(u)}$ and $\Phi^{(u)}$ belonging to the system and the bath, respectively. Explicit expressions for these operators can be obtained from a Taylor expansion of the global potential energy surface. In the following we will pick only those terms which appear to be most relevant for the envisaged relaxation dynamics in the present system. Our choice is guided by the

"rule" that only lowest-order terms for a particular mechanism should be taken into account (see also refs 39 and 40). The simplest contribution to H_{SB} is bilinear, i.e., $\propto Q_i Z_\xi$. It is responsible for one quantum transitions in system and bath. This term will be important for relaxation involving the low-frequency mode ν_1 only since the solvent does not support modes in the frequency range of the ν_{50} and ν_{29} transitions. Second, we include a term $\propto Q_i^2 Z_\xi$ which allows us to consider the effect of pure dephasing. Finally, to model the experimentally observed time scale of 400 fs for the ν_{50} population relaxation it will be necessary to consider multiquantum transitions in the bath involving intramolecular plus solvent modes. This follows from our previous observation that efficient intramolecular energy distribution is hindered by the lack of efficient resonant transitions.[30,31] Inspection of Table 1 suggests that a fourth-order process, $\propto Q_i q_m q_n Z_\xi$, could be responsible for fast relaxation.

To summarize, the system−bath interaction is expressed as $H_{SB} = H_{SB}^{(I)} + H_{SB}^{(II)} + H_{SB}^{(III)}$ with

$$H_{SB}^{(I)} = \sum_{i=1,29,50} \tilde{Q}_i \sum_\xi \hbar\Omega_\xi g_i^{(I)}(\xi)\tilde{Z}_\xi \tag{5}$$

$$H_{SB}^{(II)} = \sum_{i=1,29,50} \tilde{Q}_i^2 \sum_\xi \hbar\Omega_\xi g_i^{(II)}(\xi)\tilde{Z}_\xi \tag{6}$$

$$H_{SB}^{(III)} = \sum_{i=1,29,50} \tilde{Q}_i \sum_{m>n} \sum_\xi \hbar\Omega_\xi g_{i,mn}^{(III)}(\xi)\tilde{q}_m\tilde{q}_n\tilde{Z}_\xi \tag{7}$$

from which the identification of $K^{(u)}$ and $\Phi^{(u)}$ in eq 4 is straightforward. In eqs 5−7 we introduced the dimensionless coupling strengths $g_{i,...}^{(...)}(\xi)$ as well as the frequency of the ξth solvent bath mode Ω_ξ. Further, we use dimensionless coordinates according to $\tilde{Q}_i = Q_i/\lambda_i$. Below we will take $\lambda_i = (\hbar/2\omega_i)^{1/2}$ with ω_i being the fundamental transition frequency of the uncoupled mode Q_i. An analogous factor is introduced for the harmonic bath modes.

2.3. Spectral Densities. The equations of motion for the reduced density operator ρ can be written as[16]

$$\frac{\partial\rho}{\partial t} = -i[L_{sys} + L_f(t)]\rho - R\rho \tag{8}$$

with the Liouville superoperators $L_{sys}\bullet = [H_{sys},\bullet]/\hbar$ and $L_f(t)\bullet = [H_f(t),\bullet]/\hbar$. The effect of the system−bath interaction is contained in the (Redfield) relaxation superoperator R. The matrix elements of R in the basis of the eigenstates $\{|a\rangle\}$ of the system Hamiltonian H_{sys} can be expressed in terms of the damping matrix[16]

$$\Gamma_{ab,cd}(\omega) = \sum_{uu'} K_{ab}^{(u)} K_{cd}^{(u')} C_{uu'}^{(\omega)} \tag{9}$$

as

$$R_{ab,cd} = \delta_{ac}\sum_e \Gamma_{be,ed}(\omega_{de}) + \delta_{bd}\sum_e \Gamma_{ae,ec}(\omega_{ce}) - \Gamma_{ca,bd}(\omega_{db}) - \Gamma_{db,ac}(\omega_{ca}) \tag{10}$$

In eq 9, damping the Fourier transform of the bath correlation function has been introduced as

$$C_{uu'}(\omega) = \frac{1}{\hbar^2}\,\mathrm{Re}\int_0^\infty \mathrm{d}t\, e^{i\omega t}\langle\Phi^{(u)}(t)\Phi^{(u')}(0)\rangle_B \tag{11}$$

where $\langle\bullet\rangle_B$ is the expectation value with respect to the equilibrium statistical operator of the harmonic bath. Note that we have neglected the imaginary part of the damping matrix which could lead to small shifts of the transition frequencies.[16] Further it should be pointed out that the Redfield formulation of dissipation in general violates translation invariance if the system−bath coupled is nonlinear in the system coordinate. In ref 42 it was suggested to use a Hamiltonian expressed in terms of $Q_i - \langle Q_i\rangle_{eq}$ to "cure" this defect. For the present case, however, the equilibrium expectation values $\langle Q_i\rangle_{eq}$ are close to zero and we did not consider this issue in the following.

To keep the matter simple we proceed by neglecting the mixing between different contribution to H_{SB}, i.e., the damping matrix can be split into three terms:

$$\Gamma_{ab,cd}^{(I)}(\omega) = \sum_{ij} \langle a|\tilde{Q}_i|b\rangle\langle c|\tilde{Q}_j|d\rangle\, C_{ij}^{(I)}(\omega) \tag{12}$$

with

$$C_{ij}^{(I)}(\omega) = \pi\omega^2(1 + n(\omega))\hat{J}_{ij}^{(I)}(\omega) \tag{13}$$

where $\hat{J}_{ij}^{(I)}(\omega) = J_{ij}^{(I)}(\omega) - J_{ij}^{(I)}(-\omega)$. The spectral density is given by

$$J_{ij}^{(I)}(\omega) = \sum_\xi g_i^{(I)}(\xi)\, g_j^{(I)}(\xi)\delta(\omega - \Omega_\xi) \approx g_i^{(I)}\, g_j^{(I)}\, j^{(I)}(\omega) \tag{14}$$

The second line in eq 14 involves an approximation, i.e., the coupling strength has been expressed in terms of the single parameter $g_i^{(I)}$, and the new spectral density $j^{(I)}(\omega)$ is assumed to be equal for all system coordinates. This treatment is reasonable because it will turn out that it is only the low-frequency mode ν_1 which is affected by the bilinear coupling Hamiltonian.

For the quadratic coupling we obtain

$$\Gamma_{ab,cd}^{(II)}(\omega) = \sum_{ij}\langle a|\tilde{Q}_i^2|b\rangle\langle c|\tilde{Q}_j^2|d\rangle\, C_{ij}^{(II)}(\omega) \tag{15}$$

with $C_{ij}^{(II)}(\omega)$ and $J_{ij}^{(II)}(\omega)$ having the structure of eqs 13 and 14, respectively, but with the spectral density being approximated by

$$J_{ij}^{(II)}(\omega) \approx g_i^{(II)}\, g_j^{(II)}\, j^{(II)}(\omega) \tag{16}$$

which follows from a similar reasoning as in the bilinear case. For the quadratic coupling the matrix elements $\langle a|\tilde{Q}_i^2|a\rangle$ are different from zero. (In fact, for the present anharmonic system this happens already for the linear coupling but with a magnitude that is much smaller than in the quadratic case.) As a consequence matrix elements of $\Gamma^{(II)}(\omega)$ with frequency argument equal to zero contribute to the Redfield tensor. These terms are responsible for *pure dephasing*.[16] Following refs 41 and 42 we write

$$lim_{\omega\to 0}\, C_{ij}^{(II)}(\omega) = g_i^{(II)} g_j^{(II)}\,\frac{4\pi k_B T}{\hbar}\, lim_{\omega\to 0}\,\omega(j^{(II)}(\omega) - j^{(II)}(-\omega)) = g_i^{(II)}\, g_j^{(II)}\,\gamma_{pd} \tag{17}$$

Here, for simplicity we have comprised the magnitude of the pure dephasing term into the parameter γ_{pd}, which has dimensions of s^{-1}. (Note that in principle γ_{pd} should be temperature dependent.) Further, we will not take into account the two-

quantum transitions related to the off-diagonal elements of $\tilde{Q}_i^2$. This would merely affect the low-frequency mode whose relaxation, however, can be sufficiently described by $\Gamma^{(I)}(\omega)$. Nevertheless we will stick to the coupling parameters $g_i^{(II)}$ although the last line in eq 17 contains some redundancy.

Finally, we give the damping matrix for the fourth-order relaxation. It reads

$$\Gamma^{(III)}_{ab,cd}(\omega) = \sum_{ij}\langle a|\tilde{Q}_i|b\rangle\langle c|\tilde{Q}_j|d\rangle\, C^{(III)}_{ij}(\omega) \tag{18}$$

with

$$C^{(III)}_{ij}(\omega) = 8\pi \sum_{m\neq n} c^{(III)}_{i,mn} c^{(III)}_{j,mn} \frac{\exp(\hbar\omega/2k_BT)}{\sinh(\hbar\omega_m/2k_BT)\sinh(\hbar\omega_n/2k_BT)} \times$$

$$\left\{ \frac{(\omega-\omega_m-\omega_n)^2}{\sinh(\hbar(\omega-\omega_m-\omega_n)/2k_BT)}\hat{J}^{(III)}_{ij}(\omega-\omega_m-\omega_n) + \right.$$

$$\frac{(\omega-\omega_m+\omega_n)^2}{\sinh(\hbar(\omega-\omega_m+\omega_n)/2k_BT)}\hat{J}^{(III)}_{ij}(\omega-\omega_m+\omega_n) +$$

$$\frac{(\omega+\omega_m-\omega_n)^2}{\sinh(\hbar(\omega+\omega_m-\omega_n)/2k_BT)}\hat{J}^{(III)}_{ij}(\omega+\omega_m-\omega_n) +$$

$$\left. \frac{(\omega+\omega_m+\omega_n)^2}{\sinh(\hbar(\omega+\omega_m+\omega_n)/2k_BT)}\hat{J}^{(III)}_{ij}(\omega+\omega_m+\omega_n) \right\} \tag{19}$$

Here we assumed that the different bath modes are uncorrelated and that $g^{(III)}_{i,mn}(\xi) \approx g^{(III)}_i(\xi)c^{(III)}_{i,mn}$. If we neglect once again the coordinate specificity of the spectral density, we have

$$J^{(III)}_{ij}(\omega) \approx g^{(III)}_i\, g^{(III)}_j\, j^{(III)}(\omega) \tag{20}$$

This approximation appears reasonable since only the OD stretching and bending vibrations are appreciably affected by the fourth-order coupling term. Concerning the intramolecular bath modes, we will focus on modes ν_{16} and ν_{39}, which are the only modes being appreciably coupled to the OD vibration and at the same time should, in combination with a low-frequency bath mode, provide a resonant bath transition for both the ν_{50} fundamental and the ν_{29} overtone excitation. In other words, the sum in eq 19 reduces to the terms with $m = 16$ and $n = 39$. In addition we will simulate the fourth-order coupling strength by $g^{(III)}_i$ only, i.e., the $c^{(III)}_{i,mn}$ values are set to 1. This simplification reduces the number of open and otherwise unknown parameters. In practice it would be rather difficult to calculate the fourth order derivative defining $g^{(III)}_{i,mn}(\xi)$, especially because it involves the solvent bath modes.

This holds in particular for the assumed mapping of the real solvent environment onto an *effective* harmonic oscillator bath. The latter is entirely characterized by its spectral density. Since we are aiming at the description of low-frequency solvent modes we have used the standard Ohmic spectral density with a cutoff frequency $\omega_c^{(...)}$,[16,43] i.e.,

$$\omega^2 j^{(...)}(\omega) = \Theta(\omega)\omega\, \exp(-\omega/\omega_c^{(...)}) \tag{21}$$

Note that we included the factor ω^2 into the definition of the spectral density as it is usually done in the literature.

To summarize, our relaxation model is formally characterized by 12 parameters, i.e., 9 coupling strengths $g_i^{(...)}$, the scaling factor for pure dephasing γ_{pd}, and, neglecting two-quantum transitions, the two cut-off frequencies $\omega_c^{(I)}$ and $\omega_c^{(III)}$. One may argue that this is enough to fit the behavior of any system. Below we will focus on the linear absorption spectrum as well as on the relaxation and dephasing dynamics after ultrafast excitation of the OD stretching fundamental and bending overtone band. It turns out that the available parameter space can be restricted from the very beginning because the different coupling terms are operative only for certain processes/modes, e.g., the linear coupling does not affect the stretching and bending mode at all, whose behavior is strongly influenced by the fourth-order coupling. Pure dephasing, on the other hand, has an impact on all system modes.

Again we emphasize that the selection of coupling types must be seen as a compromise between having a minimum number of parameters, but still being able to describe the most relevant processes suggested from the experimental results. The additional neglect of the two-quantum transitions $\propto\langle a|\tilde{Q}_j^2|b\rangle$ as well as the related mixing term $\propto\langle a|\tilde{Q}_j^2|b\rangle\langle c|\tilde{Q}_i|d\rangle$ should mostly affect the relaxation of the low-frequency mode, which, in view of the available information, is sufficiently described by the linear relaxation and pure dephasing terms.

3. Linear Absorption Spectrum

In Figure 3 we show the stick spectrum ($P(a)$ is the thermal distribution function)

$$A^{(S)}(\omega) = \sum_{ab} P(a)|d_{ab}|^2\delta(\omega-\omega_{ab}) \tag{22}$$

as well as the condensed phase spectrum obtained using the dephasing rates $R_{ab,ab}$ calculated according to section 2.2.

$$A(\omega) = \sum_{ab} P(a)|d_{ab}|^2 \frac{R_{ab,ab}}{(\omega-\omega_{ab})^2 + R^2_{ab,ab}} \tag{23}$$

In part A of Figure 3, the stick spectrum at $T = 0$ K is given. Note that it was necessary to shift the experimental spectrum by 40 cm^{-1} in order to facilitate comparison with our model calculation. This small discrepancy could be a result of either the quantum chemical method used or of the restriction to three relevant coordinates only. The main peak at 2288 cm^{-1} is the eigenstate $|a = 35\rangle$ which is dominated by the fundamental transition of the OD stretching vibrational zero-order state (1,0,0), see Table 2. The red shift of 112 cm^{-1} as compared to the harmonic value of 2400 cm^{-1} is an indication for the anharmonicity of the OD potential in the hydrogen bond. We note in passing that the major contribution to the excited-state absorption $\nu_{50} = 1 \rightarrow 2$ is calculated to occur at 2044 cm^{-1}. However, there are at least two more transitions, namely, at 2288 cm^{-1} and at 2201 cm^{-1}, which involve a mixing of zero-order states with substantial (2,0,0) character.

In Figure 3 there are two more relevant transitions at $T = 0$ K, both being a consequence of the anharmonic terms in $V_1(Q_{50},Q_1)$ and $V_{29}(Q_{50},Q_{29})$. First, there is a combination transition to a state of (1,0,1) character, $|a = 37\rangle$ in Table 2, which is located 66 cm^{-1} above the (1,0,0) transition. Second, we observe the overtone of the bending vibration, (0,2,0), 180 cm^{-1} below the (1,0,0) transition ($|a = 29\rangle$). The energy gap between the two main peaks is in rather good agreement with the experimental value of 170 cm^{-1}.

In part B of Figure 3 we have shown the stick spectrum at $T = 300$ K, which reveals a number of transitions as a consequence of the anharmonicity of the potential energy surface. To the red of the (1,0,0) peak we observe the (0,0,1) $\rightarrow$ (1,0,0)

transition ($|a = 2\rangle \rightarrow |35\rangle$) at 2223 cm^{-1} (marked "*" in the figure). Its position together with the smaller peaks around 2200 cm^{-1}, which involve, e.g., $|a = 3\rangle \rightarrow |37\rangle$ and $|a = 4\rangle \rightarrow |40\rangle$, corresponds nicely to the weak shoulder in the experimental spectrum. This also holds for the combination transitions in the region 2350−2400 cm^{-1} (e.g., $|a = 1\rangle \rightarrow |37\rangle$, $|a = 2\rangle \rightarrow |40\rangle$). In addition an asymmetric broadening of the main peaks is discernible. It can be attributed to transitions between states where only the stretching/bending zero-order state is incremented (e.g., $|a = 3\rangle \rightarrow |40\rangle$, $|a = 2\rangle \rightarrow |31\rangle$). At least for the bending overtone transition this asymmetry is apparent also in the experimental spectrum.

Next we discuss the linear absorption spectrum in the presence of dephasing according to eq 23. The three contributions to the dephasing rate $R_{ab,ab}$ have a rather different influence on the spectrum in the considered region of the OD fundamental transition. Let us assume that realistic cut-off frequencies ω_c are in the range of 100−250 cm^{-1}. This implies that the bilinear coupling via $H_{SB}^{(I)}$ does not give a contribution for the relaxation back to the ground state. In addition it cannot trigger effectively a transition between the states $|35\rangle$ and $|29\rangle$ due to the linearity in $\{Q_i\}$. An essential feature of the experimental spectrum is the difference in the line width of the two main peaks. To some extent this is due to the fact that combination transitions are adding to the total width and that the anharmonicity leads to an asymmetry toward the red side (see above). According to eq 23, the peak heights for transitions from the ground state $|a = 1\rangle$ are proportional to $|d_{1b}|^2/R_{1b,1b}$. From part A of Figure 3 we realize that the intensity of the overtone (0,2,0) is too small compared to the fundamental (1,0,0). In the present model this is compensated if the dephasing rate $R_{1b,1b}$ for the bending overtone transition is smaller than for the stretching fundamental transition which naturally leads to a narrower overtone band as well.

First, let us discuss the effect of the fourth-order coupling $H_{SB}^{(III)}$ on the line width. Inspecting eq 19 we find the first term $\propto J_{ij}^{(III)}(\omega - \omega_m - \omega_n)$ to give the most important contribution in the considered frequency range ($\omega_n + \omega_n = 1949$ cm^{-1}). For the Ohmic spectral density and with $\omega_c^{(III)} = 250$ cm^{-1}, $C_{ij}^{(III)}(\omega)$ will not change appreciably in the interval 2100−2300 cm^{-1}. If we assume that all fourth-order coupling strengths are all identical to $g^{(III)}$, the main difference in the dephasing rates comes from the matrix elements of the system part of $H_{SB}^{(III)}$. Due to its linearity in $\{Q_i\}$, the matrix elements for the overtone transition will be generally smaller than those for the fundamental one. Therefore, $g^{(III)}$ can be fixed by comparing the relaxation time obtained after ultrafast excitation of the ν_{50} mode with the experimental value of about 400 fs;[9] the relaxation of mode ν_{29} is accordingly slower.

The pure dephasing rate, on the other hand, is proportional to matrix elements of the type $\langle a|\tilde{Q}_i^2|a\rangle$, i.e., there is no qualitative difference between the ν_{29} overtone and the ν_{50} fundamental transition. In the following we will assume that the overall dephasing time for the ν_{50} mode is about 100 fs, i.e., in the range of what has been observed for PMME-H.[12] For a given γ_{pd} this fixes $g_{50}^{(II)}$. It turns out that the same coupling strength cannot be used for the ν_{29} mode, for it gives an absorption overtone band which is much too broad, i.e., also the ratio between the heights of the two main peaks is too large. Thus we have the constraint that $g_{29}^{(II)} < g_{50}^{(II)}$.

The spectrum shown in part B of Figure 3 represents the best compromise given the additional restrictions imposed by the phase and energy relaxation dynamics discussed in the next section. While the overall agreement appears to be reasonable, details require future refinement of the model. For instance, one might think of incorporating more modes into the relevant system. According to Table 1, mode ν_8 might be a good candidate for contributing to the broadening of the fundamental via a combination transition. Also one should keep in mind that the very appearance and relative height of the bending overtone transition relies on the Fermi resonance interaction. The details of the latter could be sensitive to additional anharmonic interactions entering upon inclusion of more modes into the relevant system.

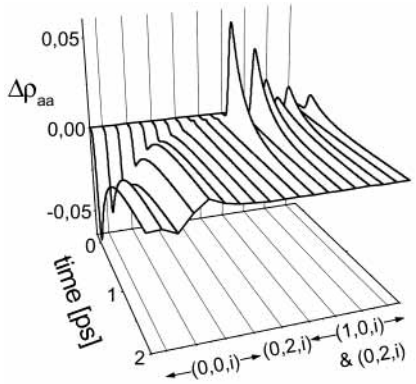

Figure 4. Population dynamics of selected eigenstates after resonant excitation of the OD stretching fundamental transition using a Gaussian shaped electric field with a fwhm of 130 fs and an amplitude of $0.001E_h/ea_B\sqrt{\text{amu}}$. The relaxation model parameters are given in the caption of Figure 3. (The states are $a = 1-8$ (ν_1 excitations), $a = 29$, 31, 34−37, 40−42, 45, and 46 (see Table 2)).

4. Dissipative Dynamics

In the following we will discuss the dynamics initiated by an external field having a Gaussian envelope of width 130 fs and being centered at $t = 0$ fs. To simplify matters we make use of the Bloch approximation to the full Redfield tensor in which the dynamics of populations and coherences are decoupled.[16] The equations of motion for ρ_{ab} have been solved using the Runge−Kutta−Verner fifth and sixth-order method with adaptive step size control. All states up to a transition frequency of 3000 cm^{-1} have been included. The following examples are intended to highlight the compatibility of the parameters used for fitting the linear absorption spectrum with the information on the relaxation and dephasing times available from the experiment.[9,12]

In Figure 4 we show the population difference $\Delta\rho_{aa}(t) = \rho_{aa}(t) - \rho_{aa}(0)$ for those eigenstates which participate appreciable in the dynamics after resonant excitation of the $\nu_{OD} = 0 \rightarrow 1$ ($|1\rangle \rightarrow |35\rangle$) transition. The population dynamics of the eigenstates follows closely from their character expressed in terms of zero-order states. The excitation goes dominantly into those states having substantial OD stretch (1,0,0) contributions. In particular the progression with respect to the ν_1 mode is populated, i.e., states $|35\rangle$, $|37\rangle$, $|40\rangle$, $|42\rangle$, and $|46\rangle$ (cf. Table 2). The T_1-type population relaxation rates for these states, i.e., $1/R_{aa,aa}$, are in the range between 300 and 350 fs as documented in Table 2. We have estimated the overall relaxation time from the initial decay of the total population dynamics of all (1,0,0) and (0,2,0) type excited states to be about 400 fs which is in agreement with the experiment.[9] The slight difference with respect to the individual relaxation times results from the excitation of bending type states whose decay times are longer but also from the competition between resonant excitation by

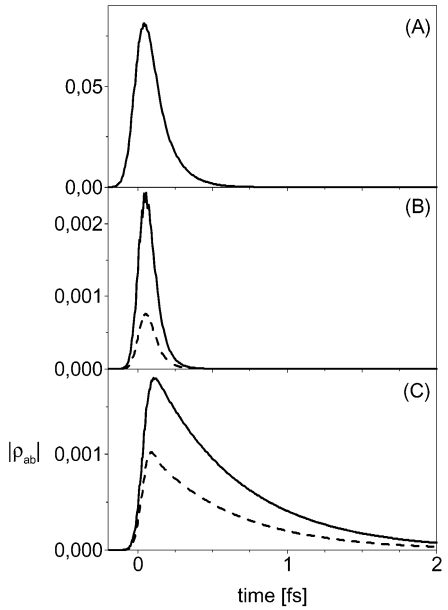

Figure 5. Coherence dynamics for the parameters of Figure 4: (A) $|\rho_{1,35}|$; (B) $|\rho_{35,37}|$ (solid), and $|\rho_{35,40}|$ (dashed); (C) $|\rho_{1,2}|$ (solid) and $|\rho_{1,3}|$ (dashed).

the laser field and simultaneous relaxation. The interplay between both processes determines the total population transfer but also the moment at which it is achieved. Typically the maximum of $\Delta\rho_{aa}(t)$ occurs during the second half of the pulse.

The depopulation of the excited states proceeds *exclusively* via the fourth-order relaxation process. The vibrational excitation of the ν_1 mode established this way in the OD ground state is distinctly nonthermal and mostly determined by processes where the ν_1 quantum number in the dominant zero-order state is conserved, i.e., $(1,0,i) \rightarrow (0,0,i)$. The relaxation of the ν_1 mode itself is governed by the bilinear coupling $H_{SB}^{(I)}$. For the chosen cut-off frequency of 100 cm^{-1} and the coupling strength $g_1^{(I)} = 0.01$, the time scale for thermalization amounts to several picoseconds, see Table 2. In the experiment[9] a slow relaxation component of 20 ps was observed and attributed to vibrational cooling. Because our gas-phase simulations[30] indicated that on this long time scale the excitation energy is likely to be shared among several low-frequency mode a quantitative comparison between the present model and the experiment appears to be not appropriate at this point.

The most intriguing aspect of the experiment[9] has been the observation of an oscillatory modulation of the IR pump−probe signal. This feature was assigned to originate from the anharmonic coupling to a low-frequency mode which modulates the strength of the H-bond.[9,29,30] Within the reduced density matrix formalism the coherent evolution of the relevant system can be rigorously investigated in terms of the off-diagonal elements of ρ_{ab}. First, let us focus on the coherence related to the ν_{50} excitation, i.e., $\rho_{1,35}$, which is shown in part A of Figure 5. The dephasing of $\rho_{1,35}$ is determined by $R_{1,35,1,35}$ which gives a total dephasing time (T_2-like) of 102 fs, see Table 2. A value of about 100 fs has been set as a goal in our fitting procedure which had to be accomplished simultaneously with the requirement for a 400 fs population relaxation and for a reasonable agreement with the absorption line shape. In Table 2 we also report the contributions to the coherence dephasing, $R^*_{a1,a1}$, which are solely due to the pure dephasing coupling in $H_{SB}^{(II)}$ (T_2-like). Our parameters suggest that the dephasing is dominated by pure dephasing, the time scale of the latter being 121 fs in the present

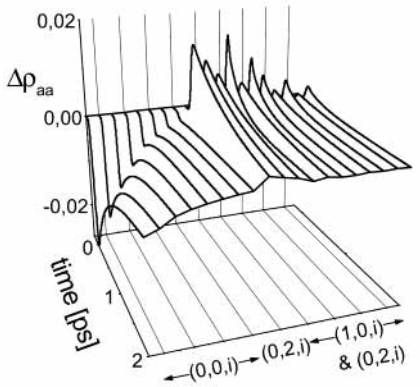

Figure 6. Same as Figure 4 but for excitation of the bending overtone transition.

case. Note that such ultrafast dephasing times for H-bonded system have been reported from four-wave-mixing experiments on PMME-H[12] and HOD/D_2O.[11]

Let us turn to the coherences with respect to the ν_1 mode. In Figure 5 we show $|\rho_{35,37}|$ and $|\rho_{35,40}|$, i.e., those matrix elements describing coherences within the vibrational progression building upon the OD fundamental transition (cf. Table 2). In terms of the Redfield tensor elements these coherences decay very rapidly on a time scale of 60 and 61 fs, respectively. The dominating pure dephasing contribution is 69 and 75 fs. Note that also the coherence with respect to the ground state decays on this time scale via the pure dephasing mechanism (Table 2). This suggests that the damped oscillations observed in ref 9 are most likely due to coherent dynamics in the OD stretch and bending ground state. This can be clearly seen from part C of Figure 5 where the ν_1 coherences $|\rho_{1,2}|$ and $|\rho_{1,3}|$ are plotted. According to Table 2 the coherence decay times being dominated by pure dephasing are about 600 fs. In fact the coupling constant $g_1^{(II)}$ has been chosen such as to give a good agreement with the value estimated from the experiment.[9] Note that within the Bloch level of description there is neither coherence transfer nor conversion of populations into coherences due to the system−bath interaction.[16] In other words, the ground state coherences are established only by the interaction with the IR laser field.

So far we have considered the dynamics after excitation of the OD stretch fundamental transition. From the experimental point of view much less is known for excitation of the bending overtone transition. In fact, the excitation conditions in ref 9 where such as to excite either to the red of the OD stretch fundamental or between the two main absorption peaks. For the latter case some excitation of the bending overtone is to be expected; however, it is hard to draw any conclusions about the related relaxation and dephasing dynamics from the present data. Our choice of parameters for the coupling of the ν_{29} mode to the bath therefore is based on the linear absorption only. In section 3, however, we put forward the argument that for the given system−bath interaction Hamiltonian $H_{SB}^{(III)}$, which can be viewed as the lowest order contribution in the system coordinate, the population relaxation of the bending overtone will always be slower than for the stretching fundamental transition. This is reflected in the relaxation times collected in Table 2 and illustrated in Figure 6. Besides the overall slowdown in the excited-state relaxation we note that progression of the ν_1 mode building upon the bending overtone is excited ($|29\rangle$, $|31\rangle$, $|34\rangle$, $|36\rangle$, ...), but also states involving mode ν_{50}. Excitation of the ν_1 progression implies the possibility of coherent vibrational motion with respect to this mode. In fact, the dynamics of the coherences looks rather similar to that

obtained for excitation of the stretching fundamental transition in Figure 5 (not shown). In other words, due to the Fermi resonance interaction between the bending overtone and the stretching fundamental transition, vibrational progressions are present for *both* transitions.

Nevertheless, we should point out that the proposed behavior of the bending overtone transition requires experimental verification coming, e.g., from two-color pump−probe experiments focusing directly on the bending vibrations. This would enable us to refine the parameters describing the relaxation of the bending mode which at this point follow solely from the fit of absorption spectrum. On the other hand, at present we cannot exclude the possibility of alternative relaxation mechanisms involving, e.g., a cascading such as $(0,2,i) \rightarrow (0,1,i) \rightarrow (0,0,i)$. For example, using a linear coupling model, Rey and Hynes[35] determined the pathway for the vibrational relaxation of HOD in D_2O to involve the first overtone and fundamental bending transitions.

Summary

With the advent of ultrafast laser source in the mid-IR it became possible to gain insight into the dynamical processes which are normally hidden under broad condensed phase spectra of intramolecular hydrogen bonds. The available knowledge about dephasing and relaxation time scales requires to go beyond the theoretical level of simple model potentials supplemented by ad hoc dephasing rates. In addition the observation of coherent dynamics demands for a rigorous quantum mechanical treatment of the relevant degrees of freedom.

In the present contribution we have combined information from quantum chemical calculations of the normal modes and anharmonic couplings in carboxy-deuterated *o*-phthalic acid monomethylester to establish a microscopic system−bath model which was treated with the formalism of the reduced density matrix. It was shown how a consistent set of parameters characterizing the system−bath interaction can be obtained by combining information from stationary IR absorption and ultrafast pump−probe and four-wave-mixing spectroscopy. For the considered system we arrived at the following conclusions:

- The double peak structure of the linear absorption spectrum results from a Fermi resonance interaction between the OD stretching fundamental and the bending overtone transition. The line widths which mask the details of the underlying stick spectrum are determined by pure dephasing and fourth-order relaxation processes.
- The ultrafast population relaxation after excitation of the OD stretching fundamental transition can be explained with the help of a fourth-order mechanism including two intramolecular modes plus a solvent phonon. For the relaxation of the bending overtone excitation we predict a slower time scale based on coupling matrix arguments.
- The dephasing of the OD stretching fundamental transition can take place on a time scale of 100 fs and is mostly determined by a pure dephasing process.
- As a consequence of the Fermi resonance vibrational progressions exist for the OD stretching fundamental as well as for the bending overtone transition. Therefore an ultrashort laser pulse will be able to excite a coherent wave packet with respect to the low-frequency vibration whose dynamics modulates the hydrogen bond. Within the present model, however, the dephasing of these coherences in the OD excites state is very rapid. On the other hand, the low-frequency vibrational coherences created by the laser pulse in the OD ground state can persist for about 2 ps. The overall thermalization of this mode can take place on an even longer time scale.

These results extend our previous gas-phase studies[29−31] and provide a microscopic picture for the essential experimental findings of Stenger et al.[9] A more detailed comparison between theory and experiment would require, e.g., calculating nonlinear-IR response functions.[45] Further testing of the model as well as its future refinement, for instance, with respect to the choice of he possible relaxation processes, has to await the availability of new experimental data scrutinizing, for instance, the dynamics of the bending vibration.

Acknowledgment. This work has been supported by the Deutsche Forschungsgemeinschaft through the Sfb450 and by the Fonds der Chemischen Industrie. The author gratefully acknowledges stimulating discussions with J. Dreyer, T. Elsaesser, P. Hamm, D. Madsen, E. Nibbering, and J. Stenger from the Max Born Institute Berlin and H. Naundorf (FU Berlin).

Note Added after ASAP Posting. This article was released ASAP on 7/20/2002 with four entries missing in Table 2. The correct version was posted on 7/22/2002.

References and Notes

(1) Jeffrey, G. A. *An Introduction to Hydrogen Bonding*; Oxford University Press: New York, 1997.
(2) Graener, H.; Seifert, G.; Laubereau, A. *Phys. Rev. Lett.* **1991**, *66*, 2092.
(3) Woutersen, S.; Emmerichs, U.; Bakker, H. J. *Nature* **1997**, *278*, 658.
(4) Laenen, R.; Simeonides, K. *J. Phys. Chem. A* **1998**, *102*, 7207.
(5) Hamm, P.; Lim, M.; Hochstrasser, R. M. *Phys. Rev. Lett.* **1998**, *81*, 5326.
(6) Nienhuys, H.-K.; Woutersen, S.; van Santen, R. A.; Bakker, H. J. *J. Chem. Phys.* **1999**, *111*, 1494.
(7) Gale, G. M.; Gallot, G.; Hache, F.; Lascoux, N.; Bratos, S.; Leicknam, J.-C. *Phys. Rev. Lett.* **1999**, *82*, 1068.
(8) Stenger, J.; Madsen, D.; Dreyer, J.; Nibbering, E. T. J.; Hamm, P.; Elsaesser, T. In *Ultrafast Phenomena XII*; Elsaesser, T., Mukamel, S., Murnane, M., Scherer, N., Eds.; Springer Series in Chemical Physics; Springer: New York, 2000; p 542.
(9) Stenger, J.; Madsen, D.; Dreyer, J.; Nibbering, E. T. J.; Hamm, P.; Elsaesser, T. *J. Phys. Chem. A* **2001**, *105*, 2929.
(10) Madsen, D.; Stenger, J.; Dreyer, J.; Nibbering, E. T. J.; Hamm, P.; Elsaesser, T. *Chem. Phys. Lett.* **2001**, *341*, 56.
(11) Stenger, J.; Madsen, D.; Hamm, P.; Nibbering, E. T. J.; Elsaesser, T. *Phys. Rev. Lett.* **2001**, *87*, 027401.
(12) Stenger, J.; Madsen, D.; Dreyer, J.; Hamm, P.; Nibbering, E. T. J.; Elsaesser, T. *Chem. Phys. Lett.* **2002**, *354*, 256.
(13) Stenger, J.; Madsen, D.; Hamm, P.; Nibbering, E. T. J.; Elsaesser, T. *J Phys. Chem. A* **2002**, *106*, 2341.
(14) Madsen, D.; Stenger, J.; Dreyer, J.; Hamm, P.; Nibbering, E. T. J.; Elsaesser, T. *Bull. Chem. Soc. Jpn.* **2002**, *75*, 909.
(15) Bratos, S.; Leicknam, J. C. *J. Chem. Phys.* **1994**, *101*, 4536.
(16) May, V.; Kühn, O. *Charge and Energy Transfer Dynamics in Molecular Systems*; Wiley-VCH: Berlin, 2000.
(17) Marechal, Y.; Witkowski, A. *J. Chem. Phys.* **1968**, *48*, 3697.
(18) Rösch, N.; Ratner, M. A. *J. Chem. Phys.* **1974**, *61*, 3344.
(19) Boulil, B.; Henri-Rousseau, O.; Blaise, P. *Chem. Phys.* **1988**, *126*, 263.
(20) Boulil, B.; Dejardin, J.-L.; Ghandour, N. E.; Henri-Rousseau, O. *J. Mol. Struct. (THEOCHEM)* **1994**, *314*, 83.
(21) Robertson, G. N.; Yarwood, J. *Chem. Phys.* **1978**, *32*, 267.
(22) Henri-Rousseau, O.; Chamma, D. *Chem. Phys.* **1998**, *229*, 37.
(23) Chamma, D.; Henri-Rousseau, O. *Chem. Phys.* **1998**, *229*, 51.
(24) Witkowski, A.; Wójcik, M. *Chem. Phys.* **1973**, *1*, 9.
(25) Bratos, S. *J. Chem. Phys.* **1975**, *63*, 3499.
(26) Bratos, S.; Ratajcak, H. *J. Chem. Phys.* **1982**, *76*, 77.
(27) Henri-Rousseau, O.; Blaise, P. *Adv. Chem. Phys.* **1998**, *103*,
(28) Henri-Rousseau, O.; Blaise, P.; Chamma, D. *Adv. Chem. Phys.* **2002**, *121*, 241.
(29) Paramonov, G. K.; Naundorf, H.; Kühn, O. *Eur. J. Phys. D* **2001**, *14*, 205.

(30) Naundorf, H.; Worth, G. A.; Meyer, H.-D.; Kühn, O. *J. Phys. Chem. A* **2002**, *106*, 719.

(31) Naundorf, H.; Kühn, O. In *Femtochemistry and Femtobiology*; Douhal, A., Santamaria, J., Eds.; World Scientific: Singapore, 2002; p 438.

(32) Došlić, N.; Sundermann, K.; González, L.; Mó, O.; Giraud-Girard, J.; Kühn, O. *Phys. Chem. Chem. Phys.* **1999**, *1*, 1249.

(33) Antoniou, D.; Schwartz, S. D., *J. Chem. Phys.* **1998**, *109*, 2287, 34.

(34) Došlić, N.; J. Stare, J.; J. Mavri, J. *Chem. Phys.* **2001**, *269*, 59.

(35) Rey, R.; Hynes, J. T. *J. Chem. Phys.* **1996**, *104*, 2356. Hynes, J. T.; Rey, R. In *Ultrafast Infrared and Raman Spectroscopy*; Fayer, M. D., Ed.; Marcel Dekker: New York, 2001; p 593.

(36) Tunon, I.; Silla, E.; Millot, C.; Martins-Costa, M. T. C.; Ruiz-Lopez, M. F. *J. Phys. Chem. A* **1998**, *102*, 8673.

(37) Webb, S. P.; Agarwal, P. K.; Hammes-Schiffer, S. *J. Phys. Chem. B* **2000**, *104*, 8884.

(38) Frisch, M. J.; et al. *Gaussian 98*, (Revision A.7); Gaussian, Inc.: Pittsburgh, 1998.

(39) Marston, C. C.; Balint-Kurti, G. G. *J. Chem. Phys.* **1989**, *91*, 3571.

(40) Kenkre, V. M.; Tokmakoff, A.; Fayer, M. D. *J. Chem. Phys.* **1994**, *101*, 10618.

(41) Tokmakoff, A.; Sauter, B.; Fayer, M. D. *J. Chem. Phys.* **1994**, *100*, 9035.

(42) Reichman, D.; Silbey, R. J.; Suarez, A. *J. Chem. Phys.* **1996**, *105*, 10500.

(43) Yan, Y.; Shuang, F.; Xu, R.; Cheng, J.; Li, X.-Q.; Yang, C.; Zhang, H. *J. Chem. Phys.* **2000**, *113*, 2068.

(44) Leggett, A. J.; Chakravarty, S.; Dorsey, A. T.; Fisher, M. P. A.; Garg, A.; Zwerger, M. *Rev. Mod. Phys.* **1987**, *59*, 1.

(45) Kato, T.; Tanimura, Y. *Chem. Phys. Lett.* **2001**, *342*, 329.